Seppanen, H; Prozheev, I; Kauppinen, C; Suihkonen, S; Mizohata, K; Lipsanen, H

Effect of atomic layer annealing in plasma-enhanced atomic layer deposition of aluminum nitride on silicon

Effect of atomic layer annealing in plasma-enhanced atomic layer deposition of aluminum nitride on silicon ⓔⓟ

Heli Seppänen ✉ ⓘⒹ ; Igor Prozheev ⓘⒹ ; Christoffer Kauppinen ⓘⒹ ; Sami Suihkonen ⓘⒹ ; Kenichiro Mizohata ⓘⒹ ;
Harri Lipsanen ⓘⒹ

Check for updates

View Online   Export Citation   CrossMark

07 August 2023 07:19:48

Effect of atomic layer annealing in plasma-enhanced atomic layer deposition of aluminum nitride on silicon EP

Heli Seppänen,[1,a] Igor Prozheev,[2] Christoffer Kauppinen,[3] Sami Suihkonen,[1] Kenichiro Mizohata,[2] and Harri Lipsanen[1]

AFFILIATIONS

[1]Department of Electronics and Nanoengineering, Micronova, Aalto University, P.O. Box 13500, Aalto FI-00076, Finland
[2]Department of Physics and Helsinki Institute of Physics, University of Helsinki, P.O. Box 43, Helsinki FI-00014, Finland
[3]VTT Technical Research Centre of Finland Ltd, Espoo FI-00014, Finland

[a]Author to whom correspondence should be addressed: heli.seppanen@aalto.fi

ABSTRACT

The effect of adding an atomic layer annealing step to a plasma-enhanced atomic layer deposition process of aluminum nitride was investigated with commonly available materials. The refractive index, crystallinity, stoichiometry, and impurity concentrations were studied from films grown from trimethylaluminum and ammonia precursors at $300\,°C$ on Si(111) substrates. Additional energy provided by the atomic layer annealing step during each deposition cycle was found to enhance the crystallinity and stoichiometry and increase the refractive index and film density. A polycrystalline hexagonal film with a weak c-axis orientation was obtained on substrates with and without native oxide, which is promising for applications that require high quality films at low temperatures.

I. INTRODUCTION

Aluminum nitride (AlN) is an attractive material for a range of applications due to its characteristics: wide bandgap,[1] high refractive index,[1] piezoelectric properties,[2] low thermal expansion coefficient,[3] and high thermal conductivity.[4] It can be grown with different techniques, depending on the requirements on the film, for instance, crystallinity, orientation, and impurity concentration. Sputtering produces a film with a columnar structure and a c-axis preferred orientation, which makes it useful for different microelectromechanical systems (MEMS) applications, such as thin-film bulk acoustic resonators,[5] piezoelectric energy harvesters[6] along with microphones[7] and piezoelectric micromachined ultrasonic transducers.[8,9] The requirement on crystal quality and purity of AlN films is at a different level in high-electron-mobility transistors (HEMTs) and light-emitting diode (LED) applications, where epitaxial materials are needed. Metallo-organic vapor phase epitaxy (MOVPE) can be utilized for single crystalline material growth, and the films have an extremely low density of impurities and defects compared to sputtered AlN. However, epitaxial AlN in MOVPE is typically grown at high ($\geq 1000\,°C$) temperatures.[10] MOVPE AlN is used as a critical layer in modern semiconductor applications, such as deep ultraviolet LEDs[11,12] and HEMTs[10,13,14] for radio frequency (RF)[15,16] and power electronics.[16,17]

Atomic layer deposition (ALD) or plasma-enhanced (PE) ALD is used in applications where conformal coating or lower deposition temperatures ($< 500\,°C$) are needed, and the film quality can vary from weakly crystalline to amorphous. Such applications include memristors,[18] diffusion barriers,[19] and buffer layers.[20] Recent progress in PEALD process development has also produced piezoelectric AlN.[21,22] PEALD with an additional *in situ* atomic layer annealing (ALA) step offers a route to obtain near epitaxial film quality at low temperatures.[23] The ALA step provides additional energy from an inert plasma gas to the top atomic layer of the film during each cycle for surface reorganization and crystallization process.[24] As the energy delivered from the plasma is confined at the film surface, repeating the ALA step during each deposition cycle is essential for the enhanced crystallization.[24,25]
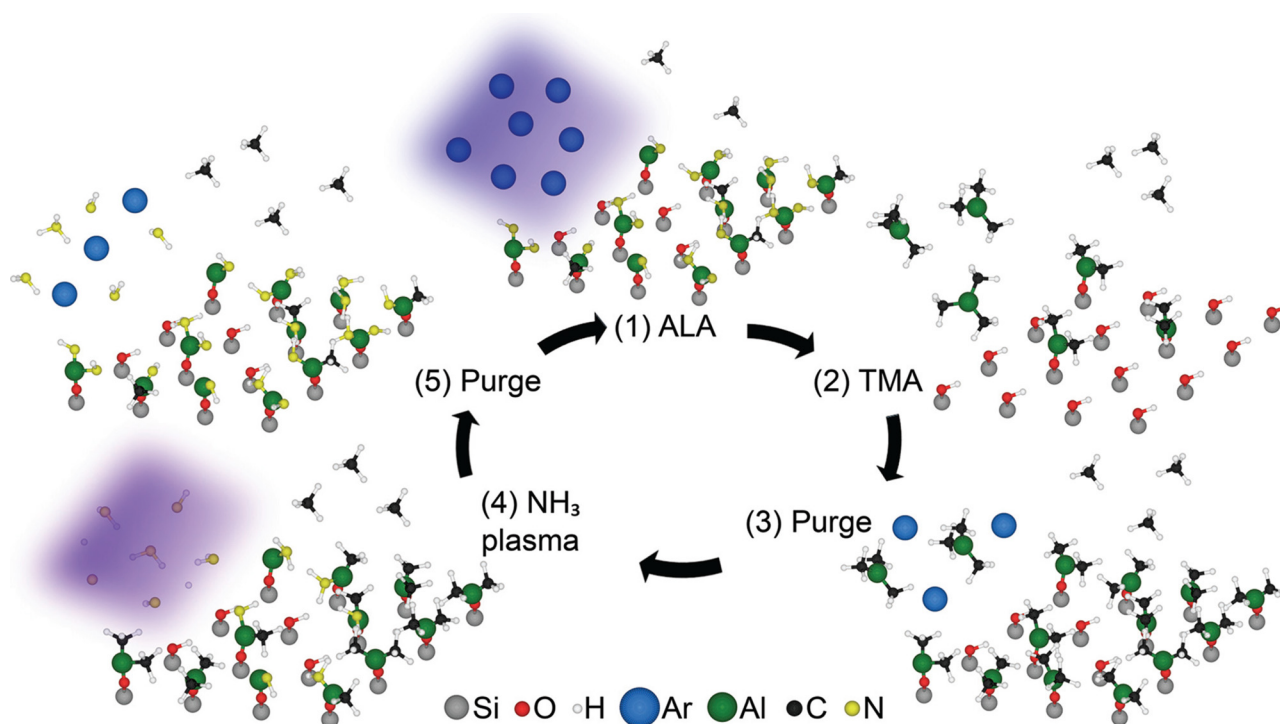
FIG. 1. Sketch of a PEALD ALA cycle with a gas flow direction from left to right. (1) Atomic layer annealing with argon plasma cleans the silicon substrate surface in the beginning of the process and later provides extra energy to the film surface to aid the crystallization process and remove impurities. (2) TMA pulse terminates the surface and releases the methane gas. Some available surface sites may remain unreacted due to methyl ligands blocking them from incoming TMA molecules. (3) Flow of an argon carrier gas purges the reaction chamber from an unreacted precursor and reaction by-products. (4) Ammonia plasma is introduced to the surface and removes methyl ligands bonded to aluminum and releases the methane gas. (5) Unreacted precursors and gaseous reaction products are purged from the reaction chamber.

PEALD ALA enables the use of AlN films in a wider variety of applications where crystalline conformal coating is needed at lower deposition temperatures on, for example, wafers, thin films, and devices with a low temperature budget. Recent reports have demonstrated PEALD ALA AlN[23] and GaN[26] on sapphire; however, silicon substrates have been overlooked in PEALD ALA research.

Silicon is a cheap and well studied substrate material that has been widely used in semiconductor research and industry for several decades. It is the key material in many commercially available applications, such as MEMS and electronics, where price, availability, and wafer size are crucial. Research on PEALD ALA grown AlN has generally concentrated on substrates that promote c-axis oriented growth[23] or on silicon with customized precursors.[27] To the best of our knowledge, a study of AlN grown with a more common approach to PEALD ALA with a thorough characterization has not been reported.

In this work, we report on the effect of adding an ALA step to a conventional PEALD process of AlN films with commonly available materials. The films are deposited on Si(111) substrates with trimethylaluminum and ammonia precursors in an industrially available reactor. The thickness and uniformity of the films are characterized using spectroscopic ellipsometry, microstructure, and crystallinity with x-ray diffraction and film composition with time-of-flight elastic recoil detection analysis. The effect of the ALA step is evaluated by comparing the results with previously grown PEALD AlN and literature data.

II. EXPERIMENT

A. Atomic layer deposition

1000 cycles of AlN were deposited on 4″ Si(111) wafers with native oxide (AlN on Si) and Si(111) with native oxide removed (AlN on HF-Si). The native oxide was removed by dipping the wafer for 20 min in buffered hydrofluoric acid (AP 90-10, Honeywell), subsequently rinsing it in de-ionized water for 20 min, and loading it straight into the Ar atmosphere. PEALD with ALA was carried out in a Beneq TFS 500 reactor with a remote capacitive 13.56 MHz RF plasma. The process temperature was 300°C, and Ar (99.9999% pure, Linde) was used as both carrier gas and plasma carrier gas. Trimethylaluminum (TMA) ($>99.5\%$ pure, Volatec) and ammonia (NH_3) (99.9999% pure, Linde) were used as precursors for AlN. A plasma power of 200 W was used for both ALA and NH_3 plasma. The carrier gas flows in the process were 150 sccm in the NH_3 line, 400 sccm to the process chamber, 50 sccm in the TMA line, and 100 sccm for the plasma gas, respectively.
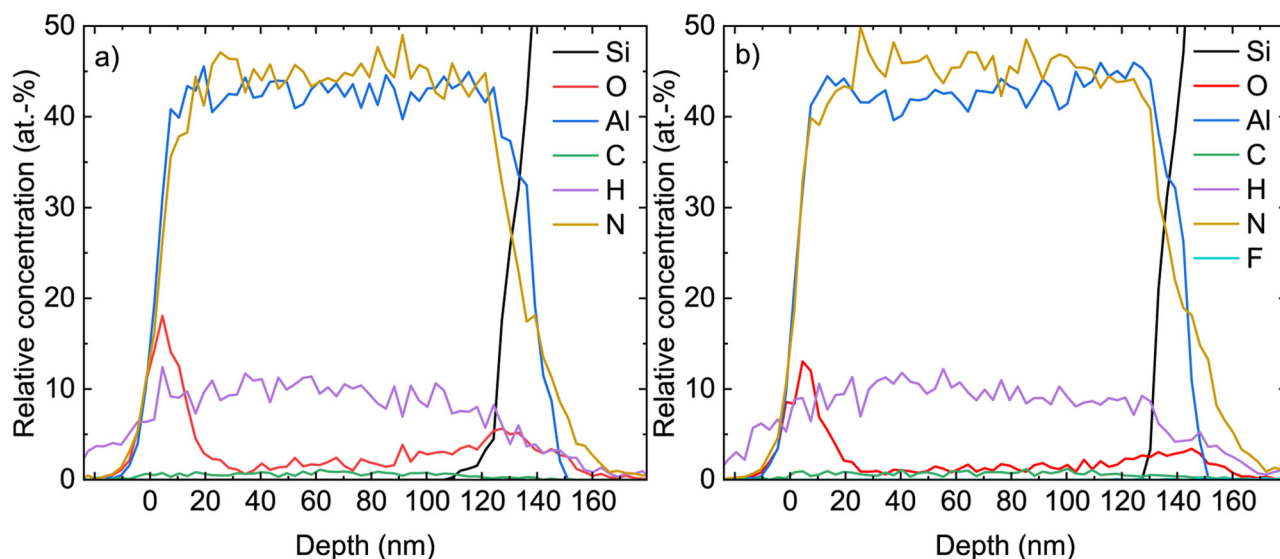
FIG. 2. Depth profiles of elements measured with TOF-ERDA of (a) AlN on Si and (b) AlN on HF-Si.

The PEALD ALA process has a five-step cycle instead of the more conventional four-step cycle, as presented in Fig. 1. The cycle begins with the ALA treatment, a 20 s Ar plasma pulse at 200 W. The purpose is to clean the sample surface during the first cycles and later provides additional energy for the film to reduce the amount of impurities and enhance the crystallization process. According to previous research, the effect of ALA is limited to the top atomic layer and is lost when it is not repeated during every deposition cycle.[24,25] The ALA step extends the process time significantly; nevertheless, the extra energy provided by the plasma is essential to reach high quality films.

The ALA step is followed by a conventional temporal PEALD cycle, where the first 0.3 s precursor pulse of TMA terminates the surface and releases methane. As pictured, unidealities, such as steric hindrance from methyl ligands blocking available surface sites, can occur during the process, and every available atom is not able to react during a cycle. During the 4 s purge, the unreacted precursor and gaseous reaction products leave the reaction chamber. Next, a 15 s pulse of NH_3 plasma with 200 W power is introduced to the surface. The plasma head is first filled with an NH_3 gas before turning on the plasma power in order to obtain a stable plasma pulse. Ideally, the plasma species remove all the methyl ligands bonded to the aluminum atoms during this step; however, this is not always the case, as will be discussed later. The unreacted precursor and gaseous reaction products leave the reaction chamber during the second purge of 6 s before the cycle starts over. Due to the tool configuration, there is a wait time of 0.1 s between ALA and TMA.

B. Film characterization

The thickness, refractive index, and uniformity were characterized with a Semilab SE-2000 spectroscopic ellipsometer with a fixed 70° angle. A visible spectrum (248.6–969.35 nm) was used for the measurement and fitting. Cauchy's equation was used as a model for fitting the data, and the results are presented at a common 632.8 nm wavelength.

A Rigaku SmartLab diffractometer was used for x-ray diffraction (XRD) measurements to evaluate the crystallinity of the films. The operating CuK_α radiation wavelengths were 1.540 593 Å (α1) and 1.544 414 Å (α2). High resolution parallel beam Ge220x2 optics were used as the optical configuration for x-ray reflectivity (XRR), grazing incidence (GI), and $\theta/2\theta$ scans. GIXRD was measured with a 0.5° incidence angle obtained from the XRR measurement. A focused beam was used for diffraction mapping with CBO-f optics and with a fully open 2D detector. A sample χ tilt and the angle of the detector were varied during the measurement. Rigaku GlobalFit was used for XRR data fitting, and the native oxides of both Si and AlN were taken into account in the fitting in addition to the AlN layer. Indexing of the reflections was made with the Inorganic Crystal Structure Database with collection codes 608628[28] and 54697.[29]

TABLE I. Concentrations of elements measured with TOF-ERDA in AlN samples grown on Si (left) and HF-Si (right). The values are provided with relative errors in units of atomic percent.

Element	AlN on Si (at. %)	AlN on HF-Si (at. %)
Al	42.68 ± 0.25	42.26 ± 0.25
N	45.04 ± 0.28	45.95 ± 0.27
H	9.88 ± 0.17	9.90 ± 0.16
C	0.70 ± 0.04	0.72 ± 0.03
O	1.70 ± 0.03	1.17 ± 0.03
F		<0.35

Time-of-flight elastic recoil detection analysis (TOF-ERDA) was used to study film composition. It was performed with a 40 MeV beam at the 5 MV tandem accelerator of the University of Helsinki. The experiment was conducted in a horizontal geometry with an incident angle on the sample surface at 16° and a forward scattering angle at 40°. The system consists of a time-of-flight telescope with two timing gates and an energy detector. The length of the telescope was 684 mm, apertures of timing gates were 12 and 18 mm in diameter, and time resolution was 150 ps. The energy detector with a resolution of 18 keV was placed at a distance of 1243 mm from the sample and used for particle mass separation. Absolute error due to statistical uncertainty in the measurements was less than 1%. The reader is addressed to Ref. 30 for a more detailed description of the setup.

III. RESULTS AND DISCUSSION

The deposited AlN film thickness, measured with a spectroscopic ellipsometer over a 4″ wafer, was on average 118 nm with 2.5% nonuniformity, which is determined by the formula

$$\frac{d_{max} - d_{min}}{d_{max} + d_{min}} \cdot 100\%, \qquad (1)$$

where d_{max} is the highest measured thickness and d_{min} the lowest. Some of the film thickness nonuniformity stems from a scarce shower head design that creates hot spots during the plasma pulse. The calculated growth rate is 1.18 Å per cycle, which is slightly less than with previously reported PEALD processes from the same TFS 500[31,32] and could indicate a moderately denser film. High temperature (> 200 °C) PEALD AlN processes have been reported

to have a lower growth rate since the plasma pulse adds smaller species to the surface while removing TMA ligands, which results in a better organized surface; thus, the vertical growth is slowed down.[33] In a PEALD ALA process, even slower growth rates can be expected as ALA removes extra ligands and impurities. The lower growth rate is in accordance with the XRR results, which reveal a growth rate of 1.16 Å measured from the middle of the wafer and is somewhat below average compared to the calculated growth rate from the spectroscopic ellipsometer results. The film density obtained from XRR is 3.25 g/cm³, which is significantly higher than for previously reported PEALD processes from the exact same reactor[31,32] with a density below 3 g/cm³ and close to the literature value of 3.255 g/cm³ for AlN.[4] The refractive index is 1.98 with 2.6% nonuniformity and higher than previously reported,[31] yet still in the polycrystalline range. Amorphous AlN has been found to exhibit refractive indexes at 1.8–1.95,[31,34] polycrystalline at 1.95–2.05,[35] and epitaxial at 2.1–2.2.[36,37] A higher hydrogen concentration in the film can lower the refractive index in PEALD films.[31]

Figure 2 shows the depth profiles of the TOF-ERDA analysis. The films are slightly nitrogen rich with the Al:N ratio of approximately 0.95, which is close to the stoichiometric value of AlN and significantly higher than in previous reports using the exact same reactor[31,32] where the ratio stays below 0.90. There is an oxygen peak at the surface of the films, indicating native oxide formation on the AlN films despite the samples were cooled down in a load-lock before exposing to ambient air. The films are stable in ambient air, as the surface oxide remains thin.

Oxygen concentration in the film is around 1.7 at. % for the sample AlN on Si and 1.17 at. % for AlN on HF-Si, which can be seen from Table I. Removing the Si surface oxide did not affect the
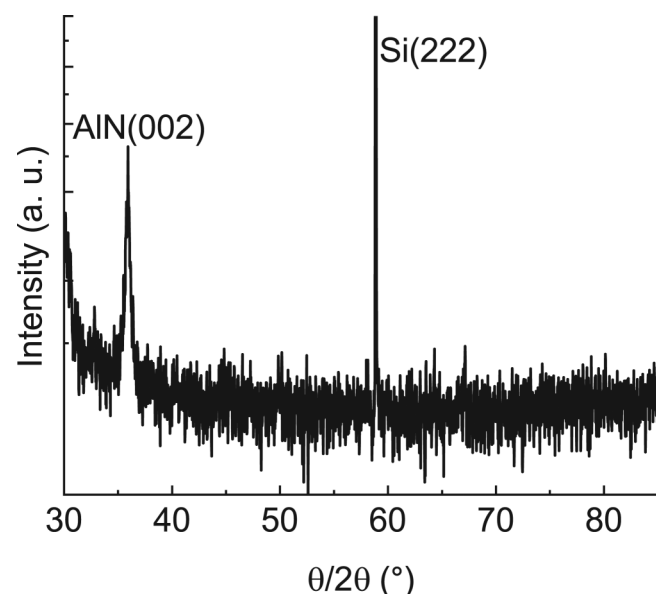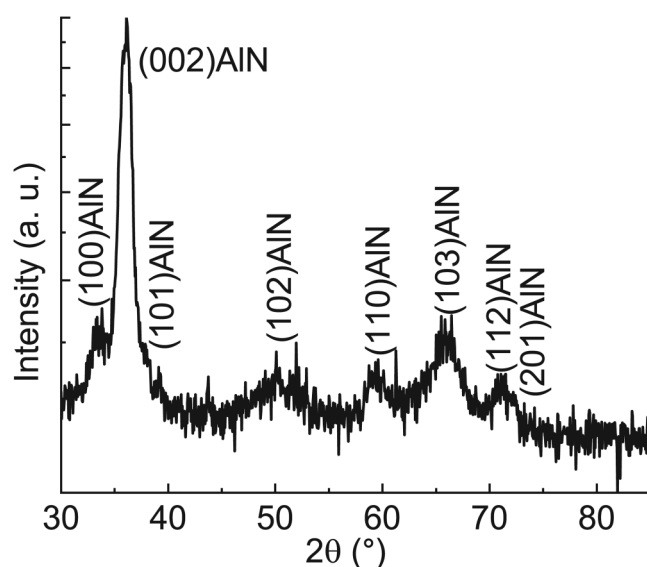
FIG. 3. θ/2θ diffractogram of AlN on Si exhibits only (002) reflection from the AlN film. The data are normalized and plotted as a square root.
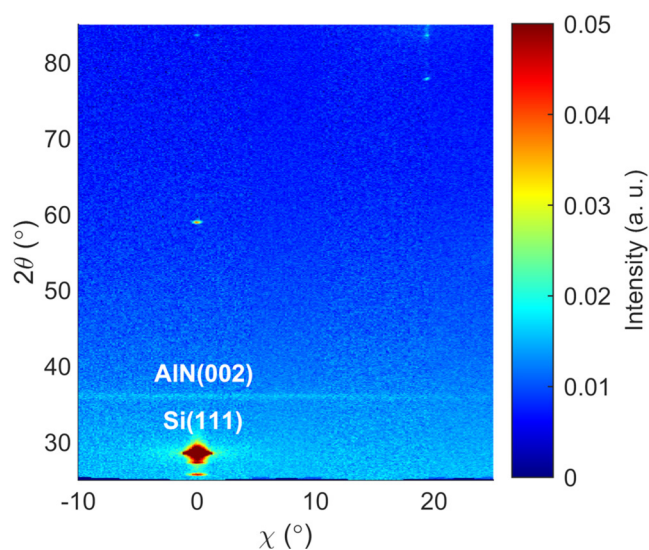
FIG. 4. Wide-area diffraction map from AlN on Si. Removing substrate native oxide did not affect the FWHM. The data are normalized and plotted as a square root.

FIG. 5. GIXRD diffractogram from AlN on Si with AlN planes indexed (Refs. 28 and 29) The data are normalized and plotted as a square root to show the smallest reflections.

TOF-ERDA results except for the part of oxygen; the amount of oxygen was lower by 0.5% throughout the film in addition to the film-substrate interface where oxygen is barely present. Sample AlN on Si was deposited before AlN on HF-Si, which means that tool condition was different during the depositions and could be a reason for the elevated amount of oxide in the film of AlN on Si. In the HF-dipped sample, there are also detectable traces of fluorine at the AlN/Si interface, which indicates that the surface is partly fluorine terminated. Despite the fact that F is detectable, the relative value is below 1% and is barely visible in Fig. 2(b). The carbon residue from most likely TMA remains at 0.7 at. %. The concentration of hydrogen is close to 10 at. %, where some of it is probably still bonded to the carbon due to an incomplete reaction of TMA, but mostly a residue from the NH_3 plasma since hydrogen remains in large amounts also in films deposited from a hydrogen-free Al precursor.[38]

Nitrogen concentration 45% is in agreement with previous reports[31,32] for films deposited at 300°C with TMA and NH_3, whereas aluminum concentration has increased significantly by 5 at. % measured with TOF-ERDA. The impurity content from carbon and hydrogen are down by 1 and 4 at. %[31,32] probably as a result of a more complete reaction of the precursors with the help of the ALA step. The lower hydrogen concentration is probably one of the reasons behind the higher refractive index. Plasma is known to restructure the surface for promoted reactivity,[39] and the ALA step can heal imperfections in the film by a momentum transfer process from the incoming ions at the impact with the surface or later through lattice vibrations.[24] The amount of impurities can also be decreased by increasing the plasma power and bias voltage;[32] however, the bias voltage in our case stayed quite low (< 5 V) during the process and is not likely to be the cause.

The oxygen concentration is higher on average by 1.2 at.-% compared to previous reports.[31,32] Possible sources could be incomplete nitridation of the chamber sidewalls or a residual water vapor in the reaction chamber originating from loading of the samples from ambient. The processes were started soon after loading of the samples, therefore leaving little time for all the ambient moisture to leave the reactor.

Diffractogram of the $\theta/2\theta$ measurement for sample AlN on Si is presented in Fig. 3. By only inspecting the crystalline quality of the film with a $\theta/2\theta$ measurement, the film seems to be (002) oriented and nanocrystalline. The wide-area XRD (WAXRD) measurement in Fig. 4, however, reveals the AlN(002) orientation with a large full width half maximum (FWHM) along the χ-axis suggesting a polycrystalline and weakly c-axis oriented film. To investigate the polycrystallinity further, a GIXRD scan was carried out. GIXRD measurement presented in Fig. 5 shows several peaks supporting the observation from the WAXRD map and indicates tilted grains. The reflections obtained from the GIXRD measurement are from a hexagonal AlN, and the presence of several peaks indicates that the layer consists of randomly oriented crystallites of hexagonal AlN with a weak c-axis orientation. The ALA treatment provides additional energy to the film during growth and has been shown in the same TFS 500 to enhance especially the c-axis orientation of the AlN film already at lower 100 W plasma powers in comparison with the film grown without the ALA step.[40] Compared to previous results,[31,32] the (002) reflection is more distinct in both $\theta/2\theta$ and GIXRD, which agrees with the fact that formation of (002) directed planes requires more energy in AlN than the other directions.[41]

Interestingly, removal of substrate native oxide did not affect the crystallization of the AlN film. Despite the higher oxygen content in the AlN on the Si sample, the FWHM for both samples in the WAXRD remained equally large (< 20 °). Previous research has shown that the silicon substrate orientation seems to not affect the crystallization on the AlN film grown with a PEALD ALA process; the film is still hexagonal and polycrystalline with a weak (002) preference grown on a (111) or (100) oriented silicon substrate.[40] This is probably also the reason why the AlN film crystallizes identically both on Si(111) with an amorphous native oxide and a bare crystalline Si(111) surface.

Residues from precursors, such as carbon and hydrogen, often stay in ALD films[42] and can affect the crystallization process.[43] As observed earlier in the film composition analysis, the amount of impurities can be lowered with the addition of energy to the surface by adding the ALA step to the PEALD cycle. Despite the prolonged cycle time, higher quality AlN with enhanced crystallinity and decreased amount of impurities open possibilities to utilize AlN in more demanding applications. Impurities, however, dwell in the AlN film in various ways, thus affecting the film properties through diverse mechanisms.

Atomic hydrogen in AlN is known to passivate defects, such as dangling bonds, and reside outside of the lattice,[44] which improves theoretical stoichiometry. The enhanced crystallinity of the AlN film probably results from the better stoichiometry compared to previous reports,[31,32] around 47 at.-% for Al and 50 at.-% for N when the amount of hydrogen is excluded. The oxygen impurities, on the other hand, act at low concentrations as point defects.[45] They are possibly bonded to the Al atoms, as formation

of Al–O–N is not energetically favorable for PEALD AlN,[46] and oxygen impurities are known to replace Al–N bonds with Al–O in a hexagonal lattice.[47] Previous studies have shown that oxygen impurities affect piezoelectric properties of AlN already below 1 at.-% and can act as electrically active defects,[48,49] which is detrimental for many AlN applications.

When the impurity concentration of carbon is higher than oxygen in AlN films, it is known to be the main source of electromechanical losses, especially at elevated temperatures.[50] Carbon impurities also increase optical absorption of AlN at the UV-C region.[51] The impurities could be avoided by, for example, using a carbon-free precursor or by optimizing the ALA process. Nitridizing the chamber walls properly and a longer wait time after sample loading for all of the ambient humidity to leave the chamber are some of the ways to reduce the amount of impurities in the film. Depending on the needs of the application, an educated choice of parameters, precursors, and an inert plasma annealing gas or a combination thereof are likely to produce a better film.

IV. CONCLUSIONS

In this work, AlN was grown with commonly available materials; the PEALD ALA process was used with TMA and NH_3 as precursors with Ar plasma annealing on Si(111) substrates. The films were characterized with spectroscopic ellipsometry, XRD, and TOF-ERDA. The ALA treatment was found to enhance the stoichiometry, crystallinity, and the c-axis orientation of the film and reduce the amount of hydrogen and carbon impurities. Removal of the native oxide did not affect the crystalline quality. The development potential and tunability of the PEALD ALA process offers alternative routes for new substrates and applications that require high quality films at low growth temperatures.

ACKNOWLEDGMENTS

AUTHOR DECLARATIONS

Conflict of Interest

The authors have no conflicts to disclose.

Author Contributions

Heli Seppänen: Conceptualization (lead); Data curation (lead); Formal analysis (lead); Investigation (lead); Methodology (lead); Project administration (lead); Validation (lead); Visualization (lead); Writing – original draft (lead); Writing – review & editing (lead). **Igor Prozheev:** Conceptualization (equal); Data curation (equal); Formal analysis (equal); Investigation (equal); Methodology (equal); Visualization (equal); Writing – original draft (equal); Writing – review & editing (equal). **Christoffer Kauppinen:** Investigation (equal); Methodology (equal); Project administration (equal); Supervision (equal); Writing – original draft (equal); Writing – review & editing (equal). **Sami Suihkonen:** Conceptualization (equal); Supervision (equal); Writing – original draft (equal); Writing – review & editing (equal). **Kenichiro Mizohata:** Formal analysis (equal); Investigation (equal); Writing – review & editing (equal). **Harri Lipsanen:** Funding acquisition (lead); Supervision (equal); Writing – review & editing (equal).

DATA AVAILABILITY

The data that support the findings of this study are available from the corresponding author upon reasonable request.

REFERENCES

[1] E. F. Schubert, *Light-Emitting Diodes*, 2nd ed. (Cambridge University Press, Cambridge, England, 2006).
[2] M.-A. Dubois and P. Muralt, Sens. Actuators A: Phys. **77**, 106 (1999).
[3] G. A. Slack and S. F. Bartram, J. Appl. Phys. **46**, 89 (1975).
[4] G. Slack, J. Phys. Chem. Solids **34**, 321 (1973).
[5] S.-H. Lee, J.-K. Lee, and K. H. Yoon, J. Vac. Sci. Technol. A **21**, 1 (2003).
[6] C. Fei, X. Liu, B. Zhu, D. Li, X. Yang, Y. Yang, and Q. Zhou, Nano Energy **51**, 146 (2018).
[7] M. D. Williams, B. A. Griffin, T. N. Reagan, J. R. Underbrink, and M. Sheplak, J. Microelectromech. Syst. **21**, 270 (2012).
[8] K. Bespalova, G. Ross, M. Paulasto-Kröckel, A. S. Thanniyil, C. Karuthedath, S. Mertin, and T. Pensala, "Temperature stability of electrode/AlScN multilayer systems for pMUT process integration," in *2020 IEEE International Ultrasonics Symposium (IUS)*, Las Vegas, NV, 7–11 September 2020 (IEEE, New York, 2020), pp. 1–4.
[9] K. Bespalova, E. Österlund, G. Ross, M. Paulasto-Kröckel, A. T. Sebastian, C. B. Karuthedath, S. Mertin, and T. Pensala, J. Microelectromech. Syst. **30**, 290 (2021).
[10] J. Lemettinen, C. Kauppinen, M. Rudzinski, A. Haapalinna, T. O. Tuomi, and S. Suihkonen, Semicond. Sci. Technol. **32**, 045003 (2017).
[11] H. Hirayama, S. Fujikawa, N. Noguchi, J. Norimatsu, T. Takano, K. Tsubaki, and N. Kamata, Phys. Status Solidi A **206**, 1176 (2009).
[12] J. Yan, J. Wang, Y. Zhang, P. Cong, L. Sun, Y. Tian, C. Zhao, and J. Li, J. Cryst. Growth **414**, 254 (2015).
[13] L. Shen *et al.*, IEEE Electron Device Lett. **22**, 457 (2001).
[14] M. Asif Khan, A. Bhattarai, J. Kuznia, and D. Olson, Appl. Phys. Lett. **63**, 1214 (1993).
[15] U. K. Mishra, L. Shen, T. E. Kazior, and Y.-F. Wu, Proc. IEEE **96**, 287 (2008).
[16] K. Hoo Teo *et al.*, J. Appl. Phys. **130**, 160902 (2021).
[17] T. Ueda, Jpn. J. Appl. Phys. **58**, SC0804 (2019).
[18] B. J. Choi, A. C. Torrezan, J. P. Strachan, P. G. Kotula, A. J. Lohn, M. J. Marinella, Z. Li, R. S. Williams, and J. J. Yang, Adv. Funct. Mater. **26**, 5290 (2016).
[19] S. Yang, J. Park, Y. Cho, Y. Lee, and S. Kim, Int. J. Mol. Sci. **23**, 13249 (2022).
[20] W.-C. Wang, M.-C. Tsai, Y.-P. Lin, Y.-J. Tsai, H.-C. Lin, and M.-J. Chen, Mater. Chem. Phys. **184**, 291 (2016).
[21] E. Österlund, H. Seppänen, K. Bespalova, V. Miikkulainen, and M. Paulasto-Kröckel, J. Vac. Sci. Technol. A **39**, 032403 (2021).
[22] T. Nguyen, N. Adjeroud, S. Glinsek, Y. Fleming, J. Guillot, P. Grysan, and J. Polesel-Maris, APL Mater. **8**, 071101 (2020).
[23] H.-Y. Shih, W.-H. Lee, W.-C. Kao, Y.-C. Chuang, R.-M. Lin, H.-C. Lin, M. Shiojiri, and M.-J. Chen, Sci. Rep. **7**, 2045 (2017).
[24] S. T. Ueda *et al.*, J. Mater. Chem. C **10**, 5707 (2022).
[25] W.-H. Lee, W.-C. Kao, Y.-T. Yin, S.-H. Yi, K.-W. Huang, H.-C. Lin, and M.-J. Chen, Appl. Surf. Sci. **525**, 146615 (2020).
[26] W.-H. Lee, Y.-T. Yin, P.-H. Cheng, J.-J. Shyue, M. Shiojiri, H.-C. Lin, and M.-J. Chen, ACS Sustain. Chem. Eng. **7**, 487 (2019).
[27] S. T. Ueda, A. McLeod, D. Alvarez, D. Moser, R. Kanjolia, M. Moinpour, J. Woodruff, and A. C. Kummel, Appl. Surf. Sci. **554**, 149656 (2021).
[28] H. Vollstädt, E. Ito, M. Akaishi, S. Akimoto, and O. Fukunaga, Proc. Jpn. Acad. Ser. B **66**, 7 (1990).
[29] W. Paszkowicz, S. Podsiadło, and R. Minikayev, J. Alloys Compd. **382**, 100 (2004).

[30]J. Jokinen, J. Keinonen, P. Tikkanen, A. Kuronen, T. Ahlgren, and K. Nordlund, Nucl. Instrum. Methods Phys. Res. B **119**, 533 (1996).

[31]M. Bosund, T. Sajavaara, M. Laitinen, T. Huhtio, M. Putkonen, V.-M. Airaksinen, and H. Lipsanen, Appl. Surf. Sci. **257**, 7827 (2011).

[32]P. Sippola *et al.*, J. Vac. Sci. Technol. A **36**, 051508 (2018).

[33]M. Miao and K. Cadien, RSC Adv. **11**, 12235 (2021).

[34]J. M. Khoshman and M. E. Kordesch, J. Non-Cryst. Solids **351**, 3334 (2005).

[35]H.-Y. Joo, H. J. Kim, S. J. Kim, and S. Y. Kim, J. Vac. Sci. Technol. A **17**, 862 (1999).

[36]X. Tang, Y. Yuan, K. Wongchotigul, and M. G. Spencer, Appl. Phys. Lett. **70**, 3206 (1997).

[37]D. Brunner, H. Angerer, E. Bustarret, F. Freudenberg, R. Höpler, R. Dimitrov, O. Ambacher, and M. Stutzmann, J. Appl. Phys. **82**, 5090 (1997).

[38]V. Rontu, P. Sippola, M. Broas, G. Ross, T. Sajavaara, H. Lipsanen, M. Paulasto-Kröckel, and S. Franssila, J. Vac. Sci. Technol. A **36**, 021508 (2018).

[39]H. B. Profijt, M. C. M. van de Sanden, and W. M. M. Kessels, J. Vac. Sci. Technol. A **31**, 01A106 (2013).

[40]H. Seppänen, I. Kim, J. Etula, E. Ubyivovk, A. Bouravleuv, and H. Lipsanen, Materials **12**, 406 (2019).

[41]J. Zhang, H. Cheng, Y. Chen, A. Uddin, S. Yuan, S. Geng, and S. Zhang, Surf. Coat. Technol. **198**, 68 (2005).

[42]M. Ritala and J. Niinistö, ECS Trans. **25**, 641 (2009).

[43]V. Brien and P. Pigeat, J. Cryst. Growth **310**, 3890 (2008).

[44]S. J. Pearton, J. C. Zolper, R. J. Shul, and F. Ren, J. Appl. Phys. **86**, 1 (1999).

[45]J. H. Harris, R. A. Youngman, and R. G. Teller, J. Mater. Res. **5**, 1763 (1990).

[46]P. Motamedi and K. Cadien, Appl. Surf. Sci. **315**, 104 (2014).

[47]M. Signore, A. Taurino, D. Valerini, A. Rizzo, I. Farella, M. Catalano, F. Quaranta, and P. Siciliano, J. Alloys Compd. **649**, 1267 (2015).

[48]M. Akiyama, T. Kamohara, K. Kano, A. Teshigahara, and N. Kawahara, Appl. Phys. Lett. **93**, 021903 (2008).

[49]L. Vergara, M. Clement, E. Iborra, A. Sanz-Hervás, J. García López, Y. Morilla, J. Sangrador, and M. Respaldiza, Diam. Relat. Mater. **13**, 839 (2004).

[50]I. Kogut *et al.*, Solid State Ion. **343**, 115072 (2019).

[51]T. Nagashima *et al.*, Appl. Phys. Express **5**, 125501 (2012).